文章编号：1001-9014(XXXX)XX-0001-08

DOI:10.11972/j.issn.1001-9014.XXXX.XX.001

Infrared spectroscopic analysis of O-H bond dynamics in one-dimensional confined water and bulk water

ZHANG Lei, Wang Tian-Qi, FAN Yan-Ping*

(College of Optical-Electrical and Computer Engineering, University of Shanghai for Science and Technology, Shanghai 200093, China)

Abstract: In sub nanometer carbon nanotubes, water exhibits unique dynamic characteristics, and in the high-frequency region of the infrared spectrum, where the stretching vibrations of the internal oxygen-hydrogen (O-H) bonds are closely related to the hydrogen bonds (H-bonds) network between water molecules. Therefore, it is crucial to analyze the relationship between these two aspects. In this paper, the infrared spectrum and motion characteristics of the stretching vibrations of the O-H bonds in one-dimensional confined water (1DCW) and bulk water (BW) in (6, 6) single-walled carbon nanotubes (SWNT) are studied by molecular dynamics simulations. The results show that the stretching vibrations of the two O-H bonds in 1DCW exhibit different frequencies in the infrared spectrum, while the O-H bonds in BW display two identical main frequency peaks. Further analysis using the spring oscillator model reveals that the difference in the stretching amplitude of the O-H bonds is the main factor causing the change in vibration frequency, where an increase in stretching amplitude leads to a decrease in spring stiffness and, consequently, a lower vibration frequency. A more in-depth study found that the interaction of H-bonds between water molecules is the fundamental cause of the increased stretching amplitude and decreased vibration frequency of the O-H bonds. Finally, by analyzing the motion trajectory of the H atoms, the dynamic differences between 1DCW and BW are clearly revealed. These findings provide a new perspective for understanding the behavior of water molecules at the nanoscale and are of significant importance in advancing the development of infrared spectroscopy detection technology.

Key words: One-dimensional confined water, infrared spectroscopy, hydrogen bonds

PACS:

一维受限水和体相水中O-H键动力学的红外光谱分析

张 磊, 王天棋, 范彦平*

(上海理工大学 光电信息与计算机工程学院,上海 200093)

摘要:在亚纳米碳纳米管中,水表现出独特的动力学特性,在红外光谱的高频区域,水分子内部氧-氢(O-H)键的伸缩振动与其氢键网络密切相关。因此,深入分析这两者间的关系至关重要。本文通过分子动力学模拟,研究了(6, 6)单壁碳纳米管(SWNT)中一维受限水(One-Dimensional Confined Water,1DCW)与体相水(Bulk water,BW)的O-H键伸缩振动的红外光谱及其运动特性,结果表明,1DCW中两个O-H键的伸缩振动在红外光谱中展现出不同的吸收峰频率。而BW的O-H键都呈现两个相同的主频率峰。进一步使用弹簧谐振子模型分析揭示,O-H键伸缩幅度的差异是导致其振动频率变化的主要因素,伸缩幅度增加导致弹簧刚性降低,进而振动频率降低。更深入的研究发现,水分子间的氢键相互作用是O-H键伸缩幅度增加和振动频率降低的根本原因。最后,通过分析H原子的运动轨迹,清楚地揭示了1DCW和BW之间的动态差异。这些发现为理解纳米尺度下水分子行为提供了新视角,并对推动红外光谱探测技术的发展具有重要意义。

关 键 词:一维受限水;氢键;红外光谱

中图分类号:O 433.4 **文献标识码**:A

Received date: 2024-06-06, **revised date**: 2024-08-30 **收稿日期**:2024-06-06,**修回日期**:2024-08-30

Foundation items:This work was supported by the Natural Science Foundation of China (51705326, 52075339).

Biography:ZHANG Lei, female, Anhui, PhD Candidate, Research on terahertz biophysics, E-mail:zlsun2001@163.com

* **Corresponding author**:E-mail: ypfan@usst.edu.cn

Introduction

Water is an indispensable substance in life, carrying out essential functions necessary for sustaining life activities [1-5]. It actively participates in many biological activities, such as metabolism, maintaining internal environmental stability, and protein structure maintenance [6-10]. Therefore, a deep understanding of the physical properties of water molecules is crucial.

In nature, most water exists in the form of free state bulk water (BW). However, in biochemical reactions and macromolecular biological functions, water often exists in the form of confined water within inorganic pores and certain protein structures, playing a key role. For example, the water channel protein Aquaporin-1 in biological organisms has been proven to efficiently transport water molecules across membranes while preventing ions from passing through [11]. In water protein channels, water molecules are arranged in a one-dimensional manner to form one-dimensional confined water (1DCW) [12]. Studies by Hummer et al. observed similar 1DCW structures and characteristics in (6, 6) single-walled carbon nanotubes (SWNT) [13]. Due to being confined to specific one-dimensional nanochannels, water molecules are connected through H-bonds in a front-to-back manner, achieving overall coordinated and orderly movement. This structure endows 1DCW with unique dynamic properties [14-16]. These studies further suggest that SWNT materials are simple to manufacture, structurally stable, and uniform, also possessing transport properties similar to biological channels. Therefore, simple nanochannels mimic complex biological channels, making artificial SWNT an ideal choice for studying biomimetic nano-confinement [17-19].

In recent years, with the capabilities of high-performance computing and large-scale data processing, scientists have conducted more precise and complex simulations and calculations of the water structure inside SWNT, discovering novel behaviors not observed on a macroscopic scale. These findings have propelled SWNT into new application prospects, such as precise water molecule control [20], seawater desalination [21], etc. Although understanding of 1DCW has increased [13,15-17], current experimental technology limitations mean that a complete understanding of its dynamic properties is still to be deepened. Infrared spectroscopy (IR) technology plays an important role in analyzing the structure and properties of materials [22-27]. In terms of analyzing the microstructure of water, IR technology provides important information on the internal structure and configuration of water molecules. By analyzing the vibrational and rotational modes of water molecules, the formation, breaking, and dynamic characteristics of H-bonds in water molecules can be inferred. Furthermore, IR technology can also be used to study the dynamic properties of water molecules, such as the rates of vibration and rotation, and interaction strength. Recent studies indicate that confined water exhibits significantly different absorption characteristics compared to bulk water in the infrared and far-infrared ranges [28-32]. Studies also show that the infrared spectrum of water molecules presents three significant absorption peaks in these infrared and far-infrared ranges. The different frequency ranges of these peaks reflect the different motion modes of water molecules. The high-frequency absorption peaks primarily originate from the stretching vibrations of the oxygen-hydrogen (O-H) bonds within water molecules [33]. Since the stretching vibrations of O-H bonds are extremely sensitive to changes in the local environment, they are often used as effective probes for detecting and analyzing the state of water molecules [34]. Additionally, the H-bond network structure between water molecules also significantly impacts the motion characteristics of water [35]. Therefore, using molecular dynamics (MD) simulation methods to further study the H-bond network and motion characteristics of 1DCW and BW, especially focusing on the high-frequency stretching vibrations of O-H bonds, is crucial for a deep understanding of the dynamic properties of water molecules in different environments.

This paper utilizes the SPC/E water model based on the MD simulation method to study the infrared spectroscopy and motion characteristics of 1DCW in (6, 6) SWNT. The results indicate significant differences in the O-H bond stretching vibration infrared spectra between 1DCW and BW. Subsequent analysis of the O-H bond length stretching changes, H-bonds, and motion trajectory diagrams reveals the fundamental reasons for the spectral differences.

1 Methods

1.1 Simulation methods

First, we establish a cubic simulation box with dimensions of 3.00 nm × 5.11 nm × 7.00 nm, as shown in Fig 1. The system contains a capless (6, 6) SWNT of 2.33 nm in length and 0.81 nm in diameter, horizontally positioned between two parallel open graphite sheets. Both the SWNT and graphite sheets are maintained in a rigid state, with the ends of the graphite forming a water-filled reservoir. We employed the flexible SPC/E water molecule model [36] and filled the system with 2524 water molecules under standard temperature and pressure conditions. The interactions between water molecules are represented by a potential energy function:

$$U\left(r_i,r_j\right) = k\frac{q_i q_j}{r_{ij}} + 4\varepsilon_{ij}\left[\left(\frac{\sigma_{ij}}{r_{ij}}\right)^{12} - \left(\frac{\sigma_{ij}}{r_{ij}}\right)^{6}\right] \quad (1)$$

The first term represents long-range electrostatic interactions, while the second term involves short-range Lennard-Jones (L-J) interactions. Here, $k = 1/(4\pi\varepsilon_0)$ represents the dielectric constant in vacuum; r_{ij} is the distance between atoms i and j; q_i is the charge on atom i; and the parameters ε_{ij} and σ_{ij} represent the values for L-J interactions. The force field parameters for our flexible SPC/E water model are detailed in Table 1. We conducted simulations using GROMACS 5.1.4 simulation software and treated interatomic interactions with the OPLS/AA force field, calculating the L-J parameters between

different atoms using the geometric averaging method. The leapfrog integration algorithm was used to solve the equations of motion for the particles, and periodic boundary conditions were employed to eliminate boundary effects. The simulation system operated under constant temperature and pressure conditions, with the system temperature maintained at 300 K using a Nose-Hoover thermostat and a temperature relaxation time set at 0.2 ps. The particle mesh Ewald method was used to handle electrostatic interactions, and the cutoff radius for electrostatic and van der Waals interactions was set at 1 nm. An initial pre-equilibration of 10 ns was conducted, followed by a 5 ns simulation. Data was collected at intervals of 1 fs, with the last 1 ns of trajectory data used for analyzing vibrational spectra and dynamic characteristics.

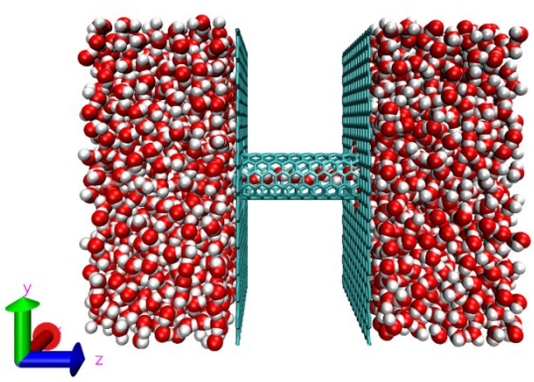

Fig. 1 Schematic of the simulation system for one-dimensional confined water (1DCW) through a single-walled carbon nanotube (SWNT) water channel: In this system, a 2.33 nm long (6, 6) SWNT is placed between two perforated graphite sheets, with water reservoirs on either side of the graphite sheets, allowing water molecules to pass through the nanotube only in the *Z* direction. In the figure, green, red, and white spheres represent carbon (C), oxygen (O), and hydrogen (H) atoms, respectively.
图1 一维受限水(1DCW)通过单壁碳纳米管(SWNT)水通道的模拟系统示意图

Table 1 Force field parameters of the flexible SPC/E water model. The ε_{ij} and σ_{ij} represent the L-J interaction parameters; q_O and q_H denote the charges of the oxygen and hydrogen atoms, respectively; θ_{H-O-H} represents the bond angle of H-O-H; r_{O-H} denotes the length of the O-H bond
表1 柔性SPC/E水模型的力场参数. εij和σij分别表示L-J作用参数;qO,qH分别表示氧原子和氢原子的电荷量;θH-O-H表示H-O-H的键角;rO-H表示O-H键的长度

Parameter	Value
σ_{O-O}/nm	0.316 6
ε_{O-O}/(kj·mol^{-1})	0.650
q_O/e	−0.848
q_H/e	0.424
θ_{H-O-H}/(°)	109.470
r_{O-H}/nm	0.100 0

1.2 Analytical method

1.2.1 Calculation of infrared spectra

In studying the infrared spectra of the O-H bond stretching vibrations in water molecules within SWNT, the required infrared spectra are calculated by performing a Fourier transform on the time autocorrelation function of the O-H bond lengths in water molecules. The mathematical expression for this calculation is as follows:

$$I(f)=\int \frac{\langle r_{O-H}(t)\cdot r_{O-H}(0)\rangle}{\langle r_{O-H}(0)\cdot r_{O-H}(0)\rangle}\cos(ft)\,dt \qquad (2)$$

In the above expression, I represents the vibrational intensity, f is the frequency, t is the time variable, and r_{O-H} is the length of the O-H bond in the water molecules.

1.2.2 Weak interaction analysis methods

Weak interaction analysis can reveal the non-covalent interactions among water molecules, such as electrostatic forces, H-bonds, and van der Waals forces. In this study, based on the initial configurations output from the MD simulations of infrared spectroscopy analysis, one water molecule is fixed while allowing other water molecules to move freely. A 1 ns MD simulation is conducted under the same conditions, yielding 1000 trajectory data frames. Utilizing these coordinate data, the average reduced density gradient (aRDG) among the water molecules is analyzed using the quantum chemical wave function analysis program Multiwfn [37]. The aRDG is calculated based on the average density gradient ($\overline{\nabla\rho(r)}$) and the average density ($\overline{\rho(r)}$) from the trajectory data, with the specific formula shown as follows:

$$aRDG(r)=\frac{1}{2(3\pi^2)^{1/3}}\frac{\left|\overline{\nabla\rho(r)}\right|}{\overline{\rho(r)}^{4/3}} \qquad (3)$$

2 Results and discussion

Firstly, we calculated the time autocorrelation functions of the O-H bond lengths in 1DCW and BW using MD simulations, and then processed these autocorrelation functions with Fourier transform to obtain the infrared spectra of the stretching vibrations. As shown in Fig 2, the gray and red curves represent the variations in the spectral intensity of the stretching vibrations of water molecule's H_1 and H_2 atoms with the O atom across different vibration frequencies, with absorption peaks primarily distributed in the 90-100 THz range. Compared to the experimentally measured overall vibration infrared spectra of the O-H bonds in BW within the 90-110 THz range, our theoretical calculations are consistent with the actual values [38]. Fig 2a displays the stretching vibration spectra of the O-H_1 and O-H_2 bonds in 1DCW, where significant differences in the vibration frequency peaks of the two are evident. The main absorption peak of the O-H_1 bond is located at 95.0 THz, while that of the O-H_2 bond is around 98.2 THz, indicating that these two O-H bonds in 1DCW exhibit different stretching vibration modes. In contrast, in BW water (as shown in Fig 2b), both O-H_1 and O-H_2 bonds exhibit two major absorption peaks, with peak frequencies and intensities that largely coincide, in-

dicating they are in the same stretching vibration mode. By comparing the infrared spectra of water in these two different environments, we find that in 1DCW, both O-H bonds have their specific vibration frequencies, whereas in BW, the vibration frequencies of the two O-H bonds vary between two peaks.

Typically, the vibrational frequency of water molecules is closely related to the internal constraints, which we liken to a spring in simple harmonic motion for the O-H bond stretching, where the force applied determines the stiffness coefficient k [39]. In simple terms, the strength of donor-acceptor interactions in the O-H bond is the main determinant of k, the interatomic distance (R_{O-H}). Based on the expression for spring harmonic vibration frequency, $f = \sqrt{k/m}$, when the interaction energy of the O-H bond is high, the spring is more rigid, meaning the stiffness coefficient k is larger, and consequently, the vibration frequency also increases. Therefore, we have conducted a detailed analysis of the O-H bond lengths and their distribution. Fig 3a and 3b show the noticeable fluctuations in the O-H_1 and O-H_2 bond lengths observed in real-time in 1DCW and BW. In 1DCW, the fluctuations in O-H_1 and O-H_2 bond lengths are distinctly different, with H_1 showing greater stretching lengths. In contrast, the fluctuations of the two O-H bonds in BW are more consistent, displaying a mix of longer and shorter bonds. As shown in Fig 3c and 3d, our statistical analysis further reveals that in 1DCW, the O-H_2 bond is shorter than the O-H_1 bond, with peak distribution lengths of 0.1005 nm and 0.1035 nm, respectively. Using the flexible SPC/E water model, the O-H bond length is 0.1000 nm (see Table 1), indicating that the O-H_2 bond in 1DCW is not affected by external forces, maintaining its vibrational characteristics, while the O-H_1 bond length has increased by 0.003 nm. Consequently, its interaction strength is reduced, the spring's rigidity is weakened, leading to a relative decrease in peak frequency. On the other hand, the distribution of the two O-H bond lengths in BW is almost identical, with peaks at about 0.1024 nm, but their distribution range is broader than in 1DCW. This indicates that the stretching amplitude of BW's O-H bonds fluctuates between longer and shorter bonds. This result further confirms that the differences in the infrared spectra of O-H bond stretching vibrations between 1DCW and BW are due to their different stretching amplitudes.

In infrared spectroscopy analysis, the high-frequency stretching vibration frequencies of the O-H bonds within water molecules exhibit a strong correlation with the H-bond network structure. To deeply understand the influence of the differences in O-H bond stretching amplitudes in 1DCW and BW on vibration frequencies, we analyzed the forces exerted by the H-bonds. Fig 4 displays a visual representation of H-bond interactions in these two different systems. Fig 4a shows that in SWNT, water molecules form a one-dimensional chain structure and are orderly connected to adjacent water molecules through H-bonds (indicated by blue discs). In 1DCW, the O-H_1 bond forms an H-bond with the oxygen atom of a neighboring water molecule, while the O-H_2 bond does not participate in H-bond formation, exhibiting free vibrations. This phenomenon is reflected in the significantly lower main peak frequency of O-H_1 in the infrared spectrum. The fundamental reason for this difference is that the O-H_1 bond, acting as an H-bond donor and being attracted by the H-bond, experiences increased stretching amplitude, reduced interaction force, weaker spring stiffness, and consequently, a lower peak frequency. On the other hand, as shown in Fig 4b, BW molecules form a tetrahedral H-bond network structure in the bulk phase, where both O-H bonds can form significant H-bonds with adjacent water molecules, distinctly different from the situation inside SWNT. These two unique H-bond network structures create different constraint envi-

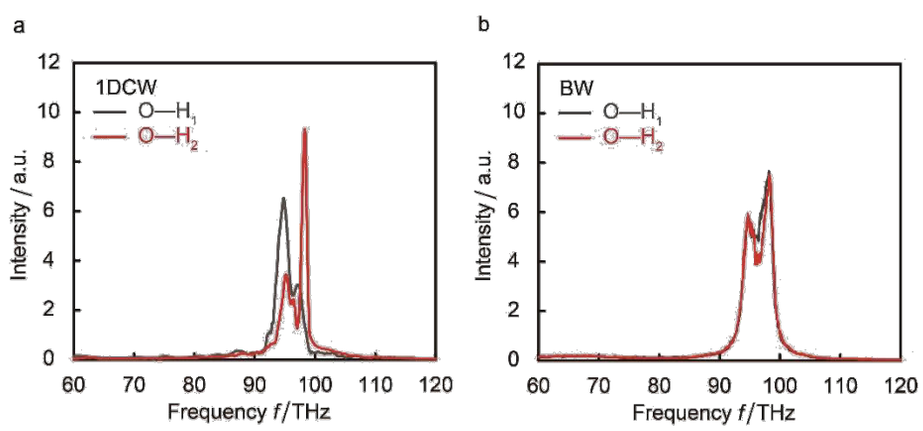

Fig. 2 Infrared spectra of O-H bond stretching vibrations in 1DCW and BW. a, b) represent the spectra of O-H bond stretching vibrations in 1DCW and BW; in both spectra, the infrared absorption peaks of the stretching vibrations appear in the frequency (f) range of 90-110 THz; the gray curve represents the stretching vibration spectrum between the H_1 atom and the O atom in water molecules (O-H_1), while the red curve represents the stretching vibration spectrum between the H_2 atom and the O atom (O-H_2)

图2 1DCW和BW中O-H键伸缩振动的红外光谱：a，b)为1DCW和BW中O-H键拉伸振动谱；在两个光谱中，拉伸振动的红外吸收峰出现在频率(□)为90~110 THz的范围内；灰色曲线为水分子中H1原子与O原子之间的拉伸振动谱(O-H1)，红色曲线为H2原子与O原子之间的拉伸振动谱(O-H2)

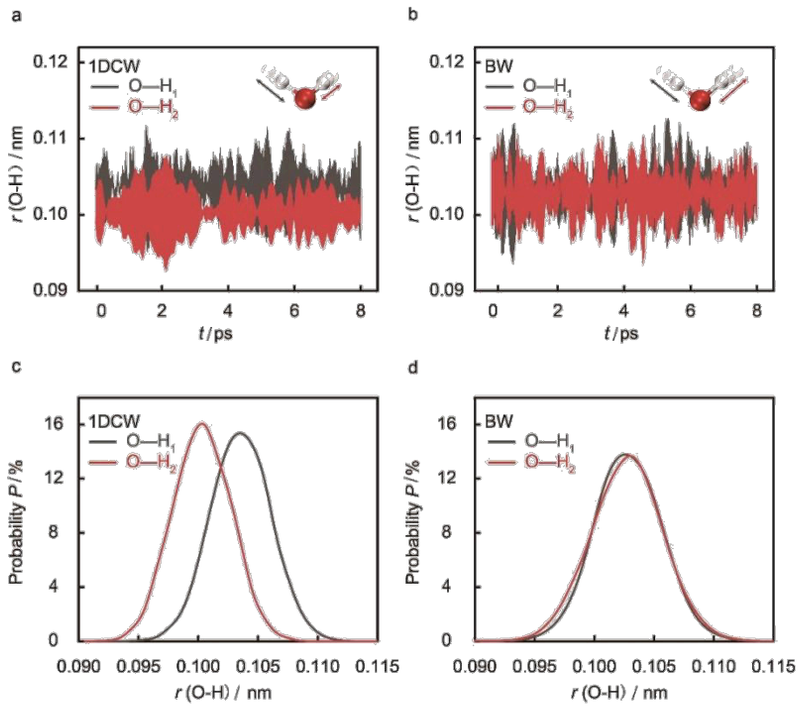

Fig. 3 Changes and distributions of O-H bond lengths over time in 1DCW and BW. a, b) Represent the stretching changes of O-H_1 and O-H_2 bond lengths over time in 1DCW and BW, respectively. Insets: the left and right sides respectively represent the stretched states of the two O-H bonds in 1DCW and BW; c, d) respectively represent the statistical distribution graphs of O-H_1 and O-H_2 bond lengths in 1DCW and BW, respectively. Herein, where the gray curve represents the distribution of the O-H_1 bond lengths in water molecules, and the red curve represents the distribution of O-H_2 bond lengths.

图3 1DCW和BW的O-H键长伸缩幅度随时间的变化和分布:a、b)分别表示了1DCW和BW中O-H1和O-H2键长度随时间的拉伸变化,并附有插图:左、右分别表示1DCW和BW中两个O-H键的拉伸状态;c、d)分别为1DCW和BW中O-H1键长和O-H2键长统计分布图,其中灰色曲线为O-H1键长在水分子中的分布,红色曲线为O-H2键长分布。

ronments, not only affecting the extent of O-H bond stretching but also leading to significant differences in vibration frequency patterns. This phenomenon profoundly reveals the key impact of H-bond network structures on molecular vibrational characteristics. In 1DCW, the O-H_1 bond involved in H-bond formation shows a lower infrared spectroscopy frequency of stretching vibrations than the O-H_2 bond, which does not form H-bonds. Meanwhile, in BW, the O-H bonds participate in both the formation and breaking of H-bonds, but due to the rapid formation and breaking, their stretching vibration frequencies fluctuate between higher and lower frequencies.

Finally, we compared the motion trajectories of water molecules in different environments. Fig 5 visually illustrates the motion characteristics of H atoms and the differences induced by their environments through two-dimensional plane projections of H atom trajectories obtained from 8 ps of MD simulations. Fig 5a and 5b reveal the differences in the motion patterns of H_1 and H_2 atoms inside SWNT in 1DCW. Due to H_1 atom′s participation in H-bonds, influenced by H-bond interactions and the spatial constraints of SWNT, its trajectory across all three planes is more concentrated, indicating its relatively slow and limited range of motion. In contrast, the H_2 atom, not involved in H-bonds, exhibits a more dispersed trajectory, especially showing a significant circular path on the XY plane, clearly indicating the free motion around the tube axis (Z-axis being the direction of the SWNT) for H atoms not involved in H-bonds inside

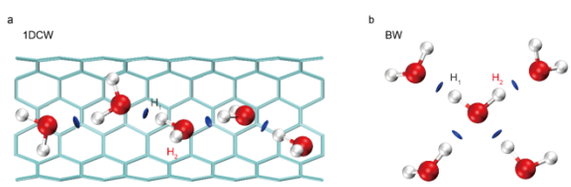

Fig. 4 The average reduced density gradient (aRDG) calculations of weak interactions in water molecules under different conditions. a) depicts the chain-like H-bond network structure in 1DCW, where only one H atom in 1DCW is involved in H-bond formation; the light blue curve represents the semi-sectional structure of a carbon nanotube, and the dark blue discs represent H-bond interactions; b) shows the tetrahedral H-bond network structure in BW, where two H atoms of a BW molecule can simultaneously form H-bond with adjacent water molecules

图4 平均约化密度函数(aRDG)计算不同环境下水分子的弱相互作用:a)为1DCW中的链状氢键网络结构,其中1DCW中只有一个H原子参与氢键的形成;浅蓝色曲线代表碳纳米管的半截面结构,深蓝色圆盘代表氢键相互作用;b)为BW中的四面体氢键网络结构,其中BW分子的两个氢原子可以同时与相邻的水分子形成氢键

SWNT. This phenomenon further illustrates how H-bond affects the vibrational characteristics of the O-H bonds, thereby causing differences in the spectra. Turning to Fig 5c and 5d, we observed no significant differences in the amplitude of motion between the two H atoms in BW. Further analysis reveals that the motion trajectories of H atoms in BW seem to be a composite of those of H_1 and H_2 atoms in 1DCW, with the amplitude between the constrained motion of H_1 and the free motion of H_2. However, the motion space for water molecules in the bulk environment far exceeds the narrow constraints of SWNT, thus allowing H atoms in the bulk to have a much larger range of activity. This finding suggests that in BW, the state of H atom motion continuously transitions between free and constrained motions, frequently undergoing the process of H-bond formation and breaking. In summary, we not only elucidate the differences in the stretching vibration infrared spectra of the O-H bonds in 1DCW and BW but also reveal the deeper mechanisms behind these differences. In 1DCW, a one-dimensional H-bond network structure is formed, while BW displays a tetrahedral H-bond network. The state of H atom motion shows clear differences due to different spatial constraints. These constraints and the interactions of H-bonds not only affect the amplitude of the O-H bond stretching vibrations but also produce unique characteristics in the infrared spectra.

3 Conclusions

In summary, this paper based on molecular dynamics simulations, analyzes the infrared spectroscopic characteristics of the O-H bonds of water in two different environments: SWNT and bulk phase. The study reveals that in 1DCW, the stretching vibration frequency of the O-H_1 bond involved in H-bond is lower than that of the O-H_2 bond which does not participate in H-bond. Conversely, in BW, the main peak frequencies of both O-H bonds are nearly identical. Further analysis showed that the stretching amplitude of the O-H_1 bond in 1DCW is significantly higher than that of the O-H_2 bond, resulting in a lower vibration frequency for O-H_1. In BW, both O-H bonds have consistent stretching amplitudes, displaying both long and short bonds, hence there are two main frequency absorption peaks. To understand more deeply the reasons for these differences in stretching amplitudes, we conducted a detailed analysis of the H-bond networks of the water molecules. In SWNT, water molecules form a one-dimensional chain structure, with only one H atom involved in H-bond, leading to differentiated stretching characteristics of the two O-H bonds. In contrast, the tetrahedral H-bond network structure in BW results in more uniform stretching amplitudes for both O-H bonds. Finally, by comparing the motion trajectories of water molecules in different environments, it was found that in 1DCW, the H_1 atom shows constrained dynamic behavior

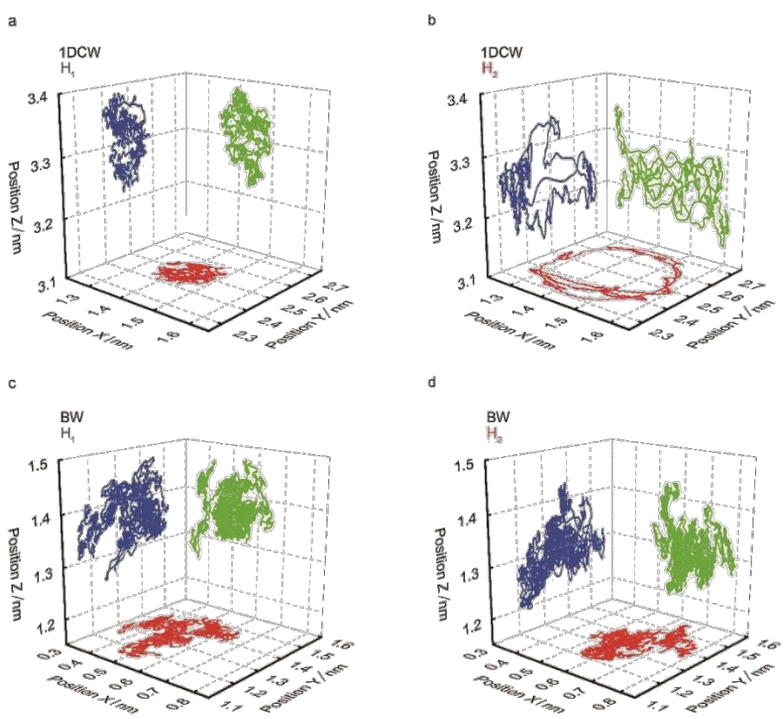

Fig. 5 Three-dimensional motion trajectories of H atoms in 1DCW and BW. a, b) respectively show the projections of the motion trajectories of H_1 and H_2 atoms in 1DCW on a two-dimensional plane; c, d) respectively represent the projections of the motion trajectories of H_1 and H_2 atoms in BW on a two-dimensional plane. These trajectories are distinguished by red, green, and blue curves, representing the motion paths of H atoms on the XY plane, XZ plane, and YZ plane respectively

图5 1DCW和BW的H原子三维运动轨迹图。a、b)分别为1DCW中H1、H2原子运动轨迹在二维平面上的投影;c, d)分别表示BW中H1和H2原子的运动轨迹在二维平面上的投影。这些轨迹用红、绿、蓝三色曲线来区分,分别代表氢原子在XY平面、XZ平面和YZ平面上的运动轨迹

due to its participation in H-bond, while H_2, not involved in H-bond, exhibits greater freedom of movement. This dynamic difference indirectly reflects the vibrational modes of the water molecule′s O-H bonds and forms specific characteristics in the infrared spectrum. However, in the tetrahedral H-bond network of BW, both H atoms are subject to similar constraints, thus their motion trajectories show no significant differences, but the state of motion continuously transitions between free and constrained, further displaying the dynamic equilibrium of H-bonds. These findings reveal the structure and dynamics of the H-bond networks of water molecules in different microenvironments and clarify how these characteristics influence the infrared spectrum of water molecules. This research deepens our understanding of the unique characteristics of molecules in diverse environments [40-41] and the fluctuation in the confinement [42-43]. Additionally, this study also provides important theoretical support for precision water modulation technologies based on infrared spectral absorption peaks [44-45], and has important implications for the study of nanofluids [46-47].

References

[1] Ball P. Water as an active constituent in cell biology [J]. *Chemical reviews*, 2008, **108**(1): 74-108.
[2] Zhou L, Wang C. Diverse phases of water molecules confined at nanoscale [J]. *Innovation Materials* 2024, **2**(1), 100049.
[3] FANG Hai-Ping. Interfacial water at microscopic level: from quasi-one-dimensional, two-dimensional confined space, to biomolecules surfaces and material surfaces [J]. *Acta Physica Sinica*(方海平。微观尺度下的水:从准一维、二维受限空间到生物以及材料表面。**物理学报**), 2016, **65**(18): 186101.
[4] Guo Y W, Qin J Y, Hu J H, *et al*. Molecular rotation-caused autocorrelation behaviors of thermal noise in water [J]. *Nuclear Science and Techniques*, 2020, **31**: 1-10.
[5] He Z, Wang J. Anti-icing strategies are on the way [J]. *The Innovation*, 2022, **3**(5), 100278.
[6] Varghese S, Kannam S K, Hansen J S, *et al*. Effect of hydrogen bonds on the dielectric properties of interfacial water [J]. *Langmuir*, 2019, **35**(24): 8159-66.
[7] Zhang Q L, Wu Y X, Yang R Y, *et al*. Effect of the direction of static electric fields on water transport through nanochannels [J]. *Chemical Physics Letters*, 2021, **762**: 138139.
[8] Zhu Z, Guo H, Jiang X, *et al*. Reversible hydrophobicity - hydrophilicity transition modulated by surface curvature [J]. *The Journal of Physical Chemistry Letters*, 2018, **9**(9): 2346-52.
[9] Akiyama R, Hirata F. Theoretical study for water structure at highly ordered surface: effect of surface structure [J]. *The Journal of chemical physics*, 1998, **108**(12): 4904-11.
[10] Gong X, Li J, Zhang H, *et al*. Enhancement of water permeation across a nanochannel by the structure outside the channel [J]. *Physical review letters*, 2008, **101**(25): 257801.
[11] Murata K, Mitsuoka K, Hirai T, *et al*. Structural determinants of water permeation through aquaporin-1 [J]. *Nature*, 2000, **407**(6804): 599-605.
[12] De Groot B L, Grubmuller H. Water permeation across biological membranes: mechanism and dynamics of aquaporin-1 and GlpF [J]. *Science*, 2001, **294**(5550): 2353-7.
[13] Hummer G, Rasaiah J C, Noworyta J P. Water conduction through the hydrophobic channel of a carbon nanotube [J]. *nature*, 2001, **414**(6860): 188-90.
[14] Holt J K, Park H G, Wang Y, *et al*. Fast mass transport through sub-2-nanometer carbon nanotubes [J]. *Science*, 2006, **312**(5776): 1034-7.
[15] Lu H, Li J, Gong X, *et al*. Water permeation and wavelike density distributions inside narrow nanochannels [J]. *Physical Review B*, 2008, **77**(17): 174115.
[16] Zhang Q L, Jiang W Z, Liu J, *et al*. Water transport through carbon nanotubes with the radial breathing mode [J]. *Physical review letters*, 2013, **110**(25): 254501.
[17] Hassan J, Diamantipoulos G, Homouz D, *et al*. Water inside carbon nanotubes: Structure and dynamics [J]. *Nanotechnology Reviews*, 2016, **5**(3): 341-54.
[18] Geng J, Kim K, Zhang J, *et al*. Stochastic transport through carbon nanotubes in lipid bilayers and live cell membranes [J]. *Nature*, 2014, **514**(7524): 612-5.
[19] Zhu Z, Chang C, Shu Y, *et al*. Transition to a superpermeation phase of confined water induced by a terahertz electromagnetic wave [J]. *The Journal of Physical Chemistry Letters*, 2019, **11**(1): 256-62.
[20] Wan R, Li J, Lu H, *et al*. Controllable water channel gating of nanometer dimensions [J]. *Journal of the American Chemical Society*, 2005, **127**(19): 7166-70.
[21] Obaidullah I. Carbon nanotube membranes for water purification: Developments, challenges, and prospects for the future [J]. *Separation and Purification Technology*, 2019, **209**: 307-37.
[22] ZHENG Zhuan-Ping, ZHAO Shuai-Yu, Liu Yu-Hang, *et al*. Terahertz spectroscopy and weak interaction analysis of cinnamic acid derivatives [J]. *Journal of Infrared and Millimeter Waves*.(郑转平,赵帅宇,刘谕杭,等。肉桂酸衍生物的太赫兹光谱及弱相互作用分析。**红外与毫米波学报**),2024,**43**(2):206-213.
[23] HE Miao, ZHOU Yi, YING Xiang-Xiao, *et al*. Si ion implantation study of InAs/GaSb type II superlattice materials[J]. *Journal of Infrared and Millimeter Waves*(何苗, 周易, 应翔霄, 等。InAs/GaSb II 类超晶格材料的Si离子注入研究。**红外与毫米波学报**), 2024, **43**(1): 15-22.
[24] ZHEN Yu-Ran, DENG Jie, BU Yong-Hao, *et al*. Recent advances in on-chip infrared polarization detection[J]. Journal of Infrared and Millimeter Waves, 2024, **43**(1): 52-62.(甄玉冉, 邓杰, 布勇浩, 等。片上红外偏振探测研究进展。**红外与毫米波学报**), 2024, **43**(1): 52-62.
[25] ZHANG Qi-Lin, WANG Rui-Feng, ZHOU T, *et al*. Molecular dynamics simulation of infrared absorption spectra of one-dimensional ordered single-file water[J]. *Acta Physica Sinica*, 2023, **72**(8): 084207.(章其林, 王瑞丰, 周同, 等。一维有序单链水红外吸收光谱的分子动力学模拟。**物理学报**), 2023, **72**(8): 084207.
[26] Fu J, Guo Z, Nie C, *et al*. Schottky infrared detectors with optically tunable barriers beyond the internal photoemission limit[J]. *The Innovation*, 2024, **5**(3), 100600.
[27] YANG Bin, LIU Zhi-Ling, HAN Lei, *et al*. Study of infrared radiation suppression on solid surfaces by spraying water film [J]. *Journal of Infrared and Millimeter Waves*(杨斌,刘志凌,韩磊,等。喷淋水膜对固体表面红外辐射抑制研究。**红外与毫米波学报**), 2024, **43**(2): 277-285.
[28] Zhu Z, Wang L, Yan S, *et al*. Enhanced water permeation through the terahertz-induced phase and diffusion transition in metal - organic framework membranes[J]. *Physical Chemistry Chemical Physics*, 2024, **26**(15): 11686-11694.
[29] Zhang Q, Zhou T, Chang C, *et al*. Ultrahigh-flux water nanopumps generated by asymmetric terahertz absorption [J]. *Physical Review Letters*, 2024, **132**(18): 184003.
[30] Zhu Z, Zhu J, Chang C, *et al*. Tunable surface wettability via terahertz electrowave controlled vicinal subnanoscale water layer [J]. *Nano Letters*, 2024, **24**(10): 3243-3248.
[31] Zhao Y, Wang L, Li Y, *et al*. Terahertz waves enhance the permeability of sodium channels[J]. *Symmetry*, 2023, **15**(2): 427.
[32] Zhu Z, Zhao Y, Chang C, *et al*. Design of artificial biomimetic channels with Na^+ permeation rate and selectivity potentially outperforming the natural sodium channel [J]. *Nano Research*, 2024, **17**: 8638-8646.
[33] Carey D M, Korenowski G M. Measurement of the Raman spectrum of liquid water [J]. *The Journal of chemical physics*, 1998, **108**(7): 2669-75.
[34] Zhang C, Khaliullin R Z, Bovi D, *et al*. Vibrational signature of water molecules in asymmetric hydrogen bonding environments [J]. *The Journal of Physical Chemistry Letters*, 2013, **4**(19): 3245-50.
[35] Lawrence C, Skinner J. Ultrafast infrared spectroscopy probes hydrogen-bonding dynamics in liquid water [J]. *Chemical physics letters*, 2003, **369**(3-4): 472-7.
[36] Berendsen H J, Grigera J R, Straatsma T P. The missing term in effective pair potentials [J]. *Journal of Physical Chemistry*, 1987, **91**(24): 6269-71.
[37] Wu P, Chaudret R, Hu X, *et al*. Noncovalent interaction analysis in fluctuating environments [J]. *Journal of chemical theory and compu-*

tation, 2013, **9**(5): 2226-2234.
[38] Heyden M, Sun J, Funkner S, *et al*. Dissecting the THz spectrum of liquid water from first principles via correlations in time and space [J]. *Proceedings of the National Academy of Sciences*, 2010, **107**(27): 12068-12073.
[39] DUAN Tong-Chuan, YAN Shao-Jian, ZHAO Yan, *et al*. Relationship between hydrogen bond network dynamics of water and its terahertz spectrum[J]. *Acta Physica Sinica*(段铜川, 闫韶健, 赵妍, 等。水的氢键网络动力学与其太赫兹频谱的关系。**物理学报**), 2021, **70**(24): 248702.
[40] Sun T, Wang L, Hu R, *et al*. Light controls edge functional groups to enhance membrane permeability[J]. *Frontiers in Physics*, 2023, **11**: 1098170.
[41] Qi C, Zhu Z, Wang C, *et al*. Anomalously low dielectric constant of ordered interfacial water[J]. *The Journal of Physical Chemistry Letters*, 2021, **12**(2): 931-937.
[42] Zhu Z, Sheng N, Fang H, *et al*. Colored spectrum characteristics of thermal noise on the molecular scale[J]. *Physical Chemistry Chemical Physics*, 2016, **18**(43): 30189-30195.
[43] Zhu Z, Sheng N, Wan R, *et al*. Intrinsic autocorrelation time of picoseconds for thermal noise in water[J]. *The Journal of Physical Chemistry A*, 2014, **118**(39): 8936-8941.
[44] Zhu Z, Chen C, Chang C, *et al*. Terahertz-light induced structural transition and superpermeation of confined monolayer water [J]. *ACS Photonics*, 2020, **8**(3): 781-6.
[45] Sun T, Zhu Z. Light resonantly enhances the permeability of functionalized membranes [J]. *Journal of Membrane Science*, 2022, **662**: 121026.
[46] Hou L, Liu X, Ge X, *et al*. Designing of anisotropic gradient surfaces for directional liquid transport: Fundamentals, construction, and applications[J]. *The Innovation*, 2023, 100508.
[47] Song Y, Xu W, Liu Y, *et al*. Achieving ultra-stable and superior electricity generation by integrating transistor-like design with lubricant armor[J]. *The Innovation*, 2022, **3**(5), 100301.